Do we know the actual magnetopause position for typical solar wind conditions?

A. A. Samsonov,[1] E. Gordeev,[1] N. A. Tsyganenko,[1] J. Šafránková,[2] Z. Němeček,[2] J. Simunek,[3] D. G. Sibeck,[4] G. Tóth,[5] V. G. Merkin,[6] J. Raeder[7]

Corresponding author: A. A. Samsonov, St.Petersburg State University, 7/9 Universitetskaya nab., St. Petersburg, 199034 Russia, (a.samsonov@spbu.ru)

[1]St. Petersburg State University, St.

Abstract. We compare predicted magnetopause positions at the subsolar point and four reference points in the terminator plane obtained from several empirical and numerical MHD models. Empirical models using various sets of magnetopause crossings and making different assumptions about the magnetopause shape predict significantly different magnetopause positions (with a scatter $> 1\ R_E$) even at the subsolar point. Axisymmetric magne-

Petersburg, Russia

[2]Charles University, Prague, Czech Republic

[3]Institute of Atmospheric Physics CAS, Prague, Czech Republic

[4]Code 674, NASA Goddard Space Flight Center, Greenbelt, Maryland, USA

[5]Department of Climate and Space, University of Michigan, Ann Arbor, Michigan, USA

[6]Johns Hopkins University Applied Physics Laboratory, Laurel, Maryland, USA

[7]Department of Physics and Space Science Center, University of New Hampshire, Durham, New Hampshire, USA

topause models cannot reproduce the cusp indentations or the changes related to the dipole tilt effect and most of them predict the magnetopause closer to the Earth than non-axisymmetric models for typical solar wind conditions and zero tilt angle. Predictions of two global non-axisymmetric models [*Lin et al.*, 2010; *Wang et al.*, 2013] do not match each other, and the models need additional verification. MHD models often predict the magnetopause closer to the Earth than the non-axisymmetric empirical models, but the predictions of MHD simulations may need corrections for the ring current effect and decreases of the solar wind pressure that occur in the foreshock. Comparing MHD models in which the ring current magnetic field is taken into account with the empirical *Lin et al.* model, we find that the differences in the reference point positions predicted by these models are relatively small for $B_z = 0$. Therefore we assume that these predictions indicate the actual magnetopause position, but future investigations are still needed.

1. Introduction

The magnetopause is the boundary between the Earth's and interplanetary magnetic fields. Space weather studies require better predictions for the magnetopause shape and position under different solar wind conditions. The magnetopause position can be roughly determined from the pressure balance between the dynamic pressure of the supersonic solar wind and the magnetic pressure of the Earth's dipole [e.g., *Chapman and Ferraro*, 1931; *Zhigulev and Romishevskii*, 1959; *Beard*, 1960; *Spreiter and Briggs*, 1962; *Mead and Beard*, 1964; *Olson*, 1969]. This method is relatively simple, but inaccurate. First, the total pressure even at the subsolar magnetopause is not exactly equal to the solar wind dynamic pressure [e.g., *Spreiter et al.*, 1966; *Samsonov et al.*, 2012]. Second, the total magnetospheric magnetic field is a superposition of magnetic fields from several current systems and the dipole field [e.g., *Tsyganenko and Andreeva*, 2015]. Later, *Sotirelis and Meng* [1999] developed a magnetopause model using the Newtonian approximation to calculate the external magnetosheath pressure and the T96 [*Tsyganenko*, 1995, 1996] magnetic field model to calculate the internal magnetospheric pressure, using a series of numerical iterations.

However, most of our knowledge about the magnetopause position comes from empirical models based on a large number of spacecraft crossings. Since *Fairfield* [1971], more than 15 empirical magnetopause models have been developed (14 of them mentioned in *Suvorova and Dmitriev* [2015]) which define the magnetopause using different sets of observations. However, with only several exceptions [*Dmitriev and Suvorova*, 2000; *Wang et al.*, 2013; *Shukhtina and Gordeev*, 2015], all the empirical models made some a priori assumptions about the magnetopause shape. For example, the well-known *Shue et al.* [1998] model assumed the functional form

$$R = R_x \left(\frac{2}{1 + \cos\theta} \right)^{\alpha} \tag{1}$$

for the magnetopause, where R is the radial distance, R_x is the position of the subsolar point, and θ is the solar zenith angle. This assumption may lead to significant errors in some regions, in particular in the cusps where the magnetopause lies closer to the Earth and the shape becomes non-axisymmetric [*Boardsen et al.*, 2000]. Recent magnetopause models [*Boardsen et al.*, 2000; *Lin et al.*, 2010; *Wang et al.*, 2013] reproduce, at least qualitatively, the cusp indentation, but both the *Boardsen et al.* [2000] and *Lin et al.* [2010] models are also based on assumed functional forms. The *Wang et al.* [2013] model uses the Support Vector Regression Machine technique, and this method is not restricted by any prescribed analytical form. However, the model includes two free parameters (γ and C) which determine the fitting procedure. The authors chose these parameters making implicit assumptions about most probable (rather smooth) magnetopause shape.

Alternatively, the magnetopause shape and position can be determined using results from global MHD simulations [e.g., *Elsen and Winglee*, 1997; *Garcia and Hughes*, 2007; *Lu et al.*, 2011]. Contrary to empirical models, the pressure balance condition in this approach is satisfied at every point, and the magnetopause shape is always non-axisymmetric. But the global MHD models do not include properly all magnetospheric current systems, in particular the ring current, therefore the magnetopause position derived from MHD solutions may also be inaccurate. In this paper, we discuss these and other factors not considered by MHD models which may influence their predictions.

Recently *Gordeev et al.* [2015] suggested a set of benchmarks for verifying global MHD codes. In particular, one of the key parameters in their tests was the magnetopause position at the subsolar point ($y = z = 0$) and $x = 0$ and $x = -15\ R_E$ planes. They compared the MHD predictions with results from the *Shue et al.* [1998] model at the subsolar point and with the *Lin et al.* [2010] model at other points. *Gordeev et al.* [2015] concluded that the MHD predictions correlate well with results from the empirical models in general, but sometimes underestimate or overestimate distances predicted by the empirical models. But they only briefly mentioned concerns about the accuracy of the empirical magnetopause models themselves. Is it really true that the empirical models are more accurate than the MHD models and which of the empirical models is better?

Our purpose now is to compare predictions of several empirical and MHD models for typical solar wind conditions. We are looking for systematic differences between axisymmetric and non-axisymmetric empirical and MHD models at reference points and will suggest explanations for these differences. We do not specifically intend to estimate the quality of different models, however we can show that predictions of some models can differ significantly from those of the majority. We investigate ways of improving the MHD models, in particular by adding the magnetic field created by the ring current. We discuss the role of the Earth's magnetic dipole tilt.

The magnetopause shape and position depend on the solar wind conditions and the Earth's dipole tilt angle, but most empirical models average magnetopause positions for different conditions using only several input parameters (usually the solar wind dynamic pressure P_{dyn} and interplanetary magnetic field B_z). Therefore we prefer to compare results from models for idealized stationary solar wind conditions rather than study some particular events with arbitrary pre-conditions when the magnetopause shape and size may be nonstationary and significantly differ from the average. We use typical solar wind conditions (see below) for which, we believe, the empirical models are most reliable.

2. Empirical and numerical models

2.1. Empirical magnetopause models

Table 1 presents a list of seven empirical and one analytical magnetopause models. The *Petrinec and Russell* [1996], *Kuznetsov and Suvorova* [1998], and *Shue et al.* [1998] models (abbreviated below as PR96, KS98, and S98 respectively) are axisymmetric, but use different analytical expressions and differ in their predictions. The analytical model of *Pudovkin et al.* [1998] (P98) was developed from the pressure balance condition at the subsolar point R_x. The P98 model uses both the well-known dependence $R_x \sim P_{dyn}^{-1/6}$ [*Mead and Beard*, 1964] and some assumptions about southward interplanetary magnetic field (IMF) penetration into the magnetosphere resulting from magnetopause reconnection. *Boardsen et al.* [2000] (B00) presented empirical models both for the high-latitude magnetopause near and behind the cusps and for the nose magnetopause. The nose magnetopause model used 290 magnetopause crossings which satisfied the criteria: latitude between $-81°$ and $81°$, and magnetic local time from 9 to 15. Contrary to the previous models noted above, these models consider the dipole tilt as one of input parameters. We will use only the nose model from *Boardsen et al.* [2000] below.

The *Lin et al.* [2010] (L10) model significantly extends the assumptions of the S98 model to obtain a three-dimensional asymmetric magnetopause surface. The model is parameterized by the solar wind dynamic and magnetic pressures, the IMF B_z, and the dipole tilt angle Ψ on the basis of 2708 magnetopause crossings in total. The three-dimensional

Wang et al. [2013] model (W13) uses the largest database, containing 15,089 magnetopause crossings. The model has no predetermined analytical form, and consequently its results for any given condition cannot be reproduced without full access to the model. *Shukhtina and Gordeev* [2015] (SG15) developed a model to determine the magnetopause position of the terminator plane in the high-latitude regions as a function of P_{dyn}, B_z and Ψ.

2.2. Global MHD models

We simulate the interaction between the solar wind and magnetosphere using the Space Weather Modeling Framework (SWMF) [*Tóth et al.*, 2005, 2012], the SWMF coupled with the Comprehensive Ring Current Model (CRCM) [*Glocer et al.*, 2013], the Lyon-Fedder-Mobarry magnetosphere-ionosphere model (LFM-MIX) [*Lyon et al.*, 2004; *Merkin and Lyon*, 2010], and the Open Geospace General Circulation Model (OpenGGCM) [*Raeder et al.*, 2001] provided by the Community Coordinated Modeling Center (http://ccmc.gsfc.nasa.gov). The resolution of the block-adaptive Cartesian grid near the magnetopause in the equatorial and terminator planes in the SWMF code is 0.125 R_E. The Cartesian grid resolution in the OpenGGCM code is similar to the SWMF, while the LFM code uses a non-Cartesian, distorted spherical mesh with a lower resolution, i.e. ~ 0.16 R_E in the radial direction and ~ 0.25 R_E in other directions in the subsolar region.

Recent global numerical models take into account the drift physics in the magnetosphere through the coupling between MHD codes and specific inner magnetospheric codes, like the Rice Convection Model (RCM) [e.g., *Wolf et al.*, 1991; *Toffoletto et al.*, 2003; *De Zeeuw et al.*, 2004; *Pembroke et al.*, 2012] or the CRCM [*Fok et al.*, 2001; *Glocer et al.*, 2013; *Meng et al.*, 2013]. In particular, the CRCM simulates the evolution of an inner magnetospheric plasma distribution that conserves the first two adiabatic invariants. The plasma pressure obtained from the CRCM simulations modifies the pressure in the MHD code. This modification self-consistently changes other MHD parameters including the magnetic field.

The low-altitude boundary of global MHD codes is located at a radial distance of $R \simeq 2-3\ R_E$. This boundary is usually a non-penetrable sphere. The density in the SWMF runs is set to 28 cm^{-3}, and in the OpenGGCM runs to 3 cm^{-3}. In the LFM runs, the radial (normal to the boundary) gradient of the density is equal to zero. *Xi et al.* [2015] compared the low-altitude boundary conditions for several global MHD models and demonstrated that these conditions may influence the accuracy of solutions. The ionospheric conductances are set to constants in the runs presented below, with Pedersen conductance $\Sigma_P = 5$ S and Hall conductance $\Sigma_H = 0$.

We fix the solar wind parameters at the outer boundary: $N = 5$ cm^{-3}, V_x=-400 km/s, $V_y = V_z = 0$ (the dynamic pressure is 1.34 nPa), $T = 2 \times 10^5$ K, $B_y = -B_x = 3.5$ nT and take different B_z. We study three stationary cases with $B_z = 0, +3, -3$ nT referred to henceforth as runs $Bz0$, $Bz+$ and $Bz-$. The dipole tilt in these three runs is set equal to zero, but we separately describe a special case with a non-zero dipole tilt angle. We usually run the codes during 3 hours with steady solar wind conditions and check that the magnetopause positions at the reference points (see below) do not change during the last hour of simulations. In some MHD models, the reference point positions (in particular, along the y-axis) may vary in time [see also *Merkin et al.*, 2013], and in this case we take averages over the last 30 minutes.

2.3. SPBU15 MHD model

We have modified the local numerical anisotropic MHD model previously described by *Samsonov et al.* [2007]; *Samsonov et al.* [2012]. The previous code used spherical coordinates and was developed only for the dayside magnetosheath, while the new code solves single-fluid 3-D MHD equations in Cartesian coordinates for the entire magnetosphere including the Earth's dipole field as explained by *Tanaka* [1994]; *Gombosi et al.* [2002]. We apply the equations in the conservative form (in particular, calculating time variations of the total energy rather than of the thermal pressure) and maintain the $\nabla \cdot \mathbf{B} = 0$ constraint using the projection scheme, i.e. solving Poisson's equation and correcting $\mathbf{B}$ after a few time steps [*Brackbill and Barnes*, 1980]. Below we will refer to this code using the working name SPBU15. We performed simulations using both the isotropic and anisotropic MHD codes (the anisotropic code calculates two thermal pressure components, $p_\perp$ and $p_\parallel$, perpendicular and parallel to magnetic field instead of only one isotropic component p), but present only the isotropic MHD results in this paper. With the given spatial resolution, we found only insignificant differences in the reference magnetopause point positions (see below) obtained by the isotropic and anisotropic codes.

The outer boundaries of the computational domain are located at $x = -30$ and $+20$ R_E and at $y, z = \pm 40$ R_E. The numerical grid is uniform in the whole region with a resolution of $0.5 \times 0.5 \times 0.5$ R_E^3. Near the Earth (at radial distances $R \leq 5$ R_E where the inner boundary is usually located), the conditions $\mathbf{V} = 0$ and $\mathbf{B_1} = 0$ (where $\mathbf{V}$ is the flow velocity and $\mathbf{B_1}$ is the external magnetic field) are applied. The density at the inner boundary equals the solar wind density, while the thermal pressure is ten times higher than the solar wind thermal pressure. Although this model cannot reproduce the inner magnetosphere, it gives reasonable results in the outer magnetosphere, in particular successfully predicting the magnetopause position.

Gombosi et al. [2002] (equations 93-97) presented a method to solve MHD equations by splitting the total magnetic field vector into the sum of two terms $\mathbf{B} = \mathbf{B_0} + \mathbf{B_1}$, where $\mathbf{B_0}$ is given analytically and thus $\nabla \cdot \mathbf{B_0} = 0$, while $\mathbf{B_1}$ is calculated by the numerical scheme. Since the subject here is the magnetopause position, $\mathbf{B_0}$ can include both the Earth's dipole field and the magnetic field of a simple model ring current (RC). Specifically, the model RC is described as a circular current loop, or a torus, of a given radius $R_{\mathrm{RC}} = 5.5\,R_E$ and finite half-thickness $D_{\mathrm{RC}} = 2\,R_E$, lying in the dipole equatorial plane and centered at the origin. The corresponding components of the RC magnetic field are described in a closed analytic form, as detailed in Appendix section of *Tsyganenko and Andreeva* [2015].

The magnitude of the RC is quantified by a single parameter ΔB, which is the disturbance field produced by the model RC at the Earth's center. We simulate the cases without the RC and with the RC yielding $\Delta B = -20$ nT in quiet conditions (here the minus sign means a negative z component) and -60 nT in moderately disturbed conditions. The parameter ΔB can thus be viewed as an approximate equivalent of the Dst^* index (corrected for the contribution from the magnetopause currents). See details on Dst^* in *Tsyganenko* [1996].

3. Results

3.1. Magnetopause shape in empirical and MHD models

The magnetopause position in MHD simulations can be determined by locating peaks in the electric current density, detecting the boundary between open and closed magnetic field lines [*Elsen and Winglee*, 1997], taking the maximum of the density gradient [*Gar-*

cia and Hughes, 2007], or tracing solar wind plasma streamlines [*Palmroth et al.*, 2003]. Magnetopause positions determined by the different methods may not coincide, especially away from the subsolar region.

Using strict magnetopause criteria is essential for automatic methods, but we can check every result by eye in case studies. In this study, we identify the magnetopause as the peak in the electric current density. This simple method fails to find the subsolar magnetopause in purely northward IMF cases, but gives reasonable results in most other cases. In empirical models, the magnetopause is primarily determined by the magnetic field rotation. Figure 1 shows the electric current density obtained by the SWMF model in the run $Bz0$. Local maxima of electric currents indicate both the magnetopause and bow shock positions, but the maximum at the dayside magnetopause is usually higher than that at the bow shock. The boundary between open and closed magnetic field lines nearly coincides with the electric current maximum in the low-latitude region sunward of the terminator ($x = 0$) plane. In the meridional plane, two high-latitude indentations on the magnetopause surface are formed above the northern and southern cusps. In the terminator plane, the magnetopause is deformed so that the cusp indentations are slightly rotated clockwise if looking from the Sun in accordance with the IMF orientation along the Parker spiral. Results from other MHD models show qualitatively similar magnetopause shapes.

We display results from three numerical (SWMF, LFM, and SPBU15 with $\Delta B = 0$) and two empirical (S98, W13) models in the equatorial and noon-meridional planes in Figure 2. In the subsolar region, the result from the S98 model nearly coincides with the predictions of the SWMF and SPBU15. The LFM model predicts the magnetopause slightly closer to the Earth, and the W13 model predicts the magnetopause at locations

$\simeq 1.5\ R_E$ larger than in the other models. The S98 model is axisymmetric, therefore it does not reproduce the cusp indentations, while the other models do predict this feature, although the size and depth of the indentations differ between each other. In the low-latitude region, the SWMF and SPBU15 predict that distances to the magnetopause are slightly smaller on the dusk than on the dawn side (compare to the axisymmetric S98 model). The only possible reason for this difference in the MHD simulations with no dipole tilt and a uniform ionospheric conductance is the Parker spiral IMF orientation. In this case, the increase of the magnetic field near the magnetopause is slightly larger downstream of the quasi-perpendicular bow shock (on the dusk flank) resulting in the asymmetric magnetopause compression. The LFM model does not predict this feature because it has been run with the solar wind condition $B_x = 0$ which is the default option used in CCMC simulations.

In general, the differences between the models in Figure 2 do not exceed 1 R_E, except for the results of the W13 model near the $z = 0$ plane and of the S98 model near and behind the cusps. In that region the difference amounts to $\simeq 1.5\ R_E$.

3.2. Magnetopause reference points

We are going to quantify the model predictions using radial distances to the magnetopause at several selected points. We find the magnetopause intersections with the x, y, and z axes, that is, the subsolar point and four points in the terminator plane. We do not address the tailward locations, because the nightside magnetopause is poorly determined in MHD simulations and the empirical models are based on much less observations in that region.

Table 2 shows the magnetopause positions (in R_E) at the reference points in the $Bz0$ case as predicted by the empirical models. R_x corresponds to the subsolar point, R_y and R_{-y} correspond to the y axis crossings on the dusk and dawn flanks respectively. As mentioned above, the MHD models predict $|R_y| < |R_{-y}|$ because the IMF is directed along the Parker spiral. From the empirical models, only the L10 model is asymmetric with respect to both the $y = 0$ and the $z = 0$ planes and predicts a similar difference ($R_y + R_{-y} = -0.5\ R_E$). The L10 model also predicts that R_z is significantly smaller than both R_y and $|R_{-y}|$, which is the effect of the cusp indentations. The differences between R_z and R_{-z} in the L10 model is small, about 0.1 R$_E$, therefore we do not discuss it.

Results of MHD models in the $Bz0$ run are collected in Table 3. The difference in R_x between the SWMF and LFM/OpenGGCM is 0.7 R_E, i.e. several times larger than the SWMF grid resolution of ≃0.125 R_E. The SWMF, SWMF-CRCM, OpenGGCM, and SPBU15 predict a moderate dawn/dusk asymmetry in the flank locations (mentioned above), i.e., a negative ($R_y + R_{-y}$) ranging from -0.8 to -0.3 R_E.

We can quantify the effect of east-west elongation (or equivalently north-south contraction) in the terminator plane related to the magnetopause indentations near the cusps using the parameter $r_{yz} = (R_y - R_{-y})/(R_z - R_{-z})$. $r_{yz} > 1$ for the asymmetric empirical and all MHD models, except the OpenGGCM. We get $r_{yz} = 1.12$ and 1.19 for the empirical L10 and W13 models, $r_{yz} = 1.11$, 1.13 and 1.10 for the SWMF, SWMF-CRCM and LFM models, respectively, and $r_{yz} = 1.05$ for the SPBU15 (without taking into account the RC).

3.3. Verification of model predictions for several selected events

Since the model predictions differ greatly, even at the subsolar point, we have selected 7 events observed by the THEMIS probes when the solar wind parameters were relatively close to the values assumed in our simulations. In particular, we choose events with a small dynamic pressure and dipole tilt angle $|\Psi| \leq 7°$ in which the magnetopause crossings occurred within 4.5 R_E from the Sun–Earth line. Table 4 summarizes information about these crossings.

Solar wind parameters for these events have been obtained from OMNIWeb (http://omniweb.gsfc.nasa.gov/) taking into account a small additional time shift (2 min) from the bow shock nose to the subsolar magnetopause. The dynamic pressure in 4 of 7 events significantly changes in 20 minutes interval centered around the shifted magnetopause crossing time. For these events, we include in Table 4 extreme dynamic pressures in the 10 min intervals prior to and after the crossing time. We also differ inward (events on 11.10.2009, 19.10.2010, 03.11.2010, 08.02.2013) and outward (30.09.2009, 25.10.2009) magnetopause crossings using signs ”>” and ”<” before *Robs* values. In event 02.11.2009, THD is close to apogee and observed an outward crossing shortly after the inward crossing. On 19.10.2010 THA observed the inward magnetopause crossing, but subsequent variations of ion and electron spectra suggest that the spacecraft stays near the magnetopause for several hours. Increases/decreases of the dynamic pressure agrees well with the inward/outward direction of the magnetopause motion.

Using the observed positions of the magnetopause crossings, the solar wind dynamic pressures and the IMF B_z, we calculate the corrected position (or two positions for variable pressure) of the subsolar point R_x^{cor} corresponding to $P_{dyn} = 1.34$ nPa. In this estimation, we assume that $R_x \sim P_{dyn}^{-1/6}$ and the magnetopause shape in the subsolar region coincides with the S98 model. Thus we take into account variations of the radial distance with P_{dyn} and solar zenith angle, but not with B_z. The IMF B_z varies between -1.1 and 5.5 nT, and the average B_z equals 2.1 nT for all events.

We get a set of estimated R_x^{cor} ranging from 10.57 to 11.88 R_E with an average $< R_x^{cor} >= 11.2 \pm 0.3$. Apparently we cannot completely rule out the effect of the dipole tilt which may significantly (at $\simeq 1$ R_E for $\Psi = 10°$) change R_x according to *Wang et al.* [2013]. In the event 11.10.2009, we have the smallest magnitude of the tilt angle $\Psi = -1.0°$ and B_z close to zero ($B_z = -0.8$ nT), and we obtain the largest $R_x^{cor} = 11.68$ R_E (average between two values). On the contrary, the smallest $R_x^{cor} = 10.57$ R_E is obtained in 08.02.2013, when the tilt angle magnitude is largest ($\Psi = -7.0°$) even for positive B_z ($B_z = 4.8$ nT).

In the estimations above, we use the solar wind dynamic pressure calculated from the proton density as given by OMNIWeb. We assume that the input parameter P_{dyn} in most empirical and all MHD models corresponds to the proton pressure. If we take into account that about 4 % of solar particles are the He^{+2} ions, the dynamic pressure should be multiplied by 1.16 that results in a larger R_x^{cor}. In the last case, $< R_x^{cor} >= 11.5 \pm 0.3$.

Plots of $R_x^{cor}(\Psi)$, $R_x^{cor}(B_z)$, and $R_x^{cor}(Dst)$ (not shown) reveal that R_x^{cor} and Ψ are anticorrelated for these events, but the dependencies $R_x^{cor}(B_z)$ and $R_x^{cor}(Dst)$ are not clearly determined due to poor statistics. We discuss these results below.

3.4. Differences between northward and southward IMF cases

It is known that the subsolar magnetopause moves earthward when the IMF rotates from northward to southward. This effect can be explained either in terms of the magnetosheath magnetic field penetration into the magnetosphere due to magnetopause reconnection [*Kovner and Feldstein*, 1973] or by reconfiguration of the magnetospheric-ionospheric currents [e.g., *Hill and Rassbach*, 1975; *Maltsev and Lyatsky*, 1975; *Pudovkin et al.*, 1986; *Sibeck et al.*, 1991; *Tsyganenko and Sibeck*, 1994], although both explanations are mutually consistent [*Pudovkin et al.*, 1998]. If the empirical models correctly determine the earthward magnetopause shift for southward IMF, we could estimate the accuracy of MHD models in predicting this shift and hence in describing the electric current reconfiguration.

We compare two cases with $B_z = +3$ nT ($Bz+$) and -3 nT ($Bz-$) with the rest of solar wind parameters being the same. Figure 3 shows the shape of the magnetopause in the $y = 0$ plane obtained in the empirical S98 and W13 models and in the numerical simulations (SWMF, LFM, and SPBU15). Tables 5 and 6 summarize the differences $\Delta R = R(Bz+) - R(Bz-)$ at the reference points for all empirical and MHD models.

In general, all models predict that the subsolar magnetopause moves earthward for southward IMF, although in some models ΔR_x does not exceed 0.2 R_E (SWMF, SPBU15), thus being hardly visible in the figure. The largest ΔR_x occur in the LFM (0.6 R_E) and OpenGGCM (0.7 R_E) numerical models, the theoretical P98 (0.95 R_E) and empirical W13 (0.89 R_E) models. Table 5 lists the average $\Delta R_x = 0.57$ R_E for seven models. We suppose that this is a reasonable measure of the southward IMF effect. Note that the SPBU15 code does not include the ionosphere and consequently cannot reproduce the magnetospheric-ionospheric currents. It seems also that the SWMF with the given spatial resolution and default numerical settings at CCMC underestimates the southward IMF effect at the subsolar point.

Now let us consider the magnetopause shape in the terminator plane. It is known that the magnetopause flaring angle increases for a southward IMF, however this effect is rather weak in the axisymmetric S98 model. In fact this effect is strongly non-axisymmetric: the MHD simulations presented below show that the distance to the magnetopause increases along the z, rather than along the y axis when IMF B_z turns southward. Note that the position of R_z (the magnetopause intersections with the z axis) should always lie tailward of the cusp, as predicted by most models. For northward IMF conditions, magnetic reconnection occurs at the high-latitude magnetopause where the boundary moves earthward. For southward IMF conditions, magnetic field lines reconnected at the dayside magnetopause convect tailward and accumulate the magnetic flux in the tail lobes [*Dungey*, 1961]. Consequently, the magnetopause radius tailward of the cusps should increase for southward IMF in agreement with previous studies [*Boardsen et al.*, 2000].

Only two empirical models, W13 and SG15, are really able to reproduce this effect predicting $\Delta R_z = -1.16$ and -0.50 R_E respectively. On the contrary, the L10 model predicts a small increase of R_z in the southward case ($\Delta R_z = 0.38$ R_E) which has no physical explanation. The W13 model contains more observations, but the SG15 model is especially designed for the high-latitude magnetopause near the terminator plane, therefore we can only guess that the real ΔR_z is between -1.16 and -0.5 R_E. The changes in the equatorial plane ΔR_y are rather small for the S98 and W13 models, but $\Delta R_y = \Delta R_z$ for the L10 model. However, we have no physical reason to suppose a significant ΔR_y between the northward and southward cases. And, to our knowledge, this problem has not been studied before. We assume that the southward IMF effect in R_y does not exceed 0.2 R_E for the assumed solar wind conditions.

Table 6 shows that all numerical models predict an increase in R_z for the southward case, but ΔR_z varies from -2.7 to -0.7 R_E depending on the model. The SWMF ($\Delta R_z = -1.3$ R_E) and the SPBU15 ($\Delta R_z = -0.7$ R_E) predictions lie closer to our expectations from empirical models for ΔR_z between -1.16 and -0.5 R_E. ΔR_y is small (0.2 R_E) in the SWMF and LFM results, but too large in the other two MHD models.

3.5. Effect of the dipole tilt

The difference between results of the axisymmetric (e.g., S98) and non-axisymmetric (B00, L10, W13) empirical models might be explained by the effect of the dipole tilt. *Wang et al.* [2013] showed that the subsolar magnetopause lies significantly farther from the Earth for zero tilt angle in their model. We calculate the magnetopause positions for the B00, L10, and W13 empirical models and the SWMF and LFM MHD models for the tilt angle $\Psi = 15°$ (for positive tilt angles, the north pole inclined sunward). Figure 4 shows the difference between the radial distances in the noon-meridional plane for the tilted and non-tilted ($\Psi = 0°$) dipoles as a function of latitude $\theta = \arctan(z/x)$.

Although all the models predict an increase in the distance to the magnetopause below the equatorial plane (but sunward of the southern cusp) and a decrease of the distance above the equatorial plane (sunward of the northern cusp) in the case $\Psi = 15°$, the magnitude of ΔR is different. It is always smaller than 0.8 R_E for the SWMF model and reaches a maximum of $\simeq 1.8$ R_E for the W13 model. Moreover, all MHD models (including the LFM model not shown in Figure 4) and the L10 empirical model, but except the B00 and W13 models predict $-0.1 < \Delta R_x < 0$ at the subsolar point. While the W13 model predicts a significant tilt effect with $\Delta R_x = -0.87$ R_E, and B00 yields an intermediate result with $\Delta R_x = -0.25$ R_E.

The dipole tilt effect can also be estimated from models which calculate the magnetopause position using the pressure balance condition. In particular, *Olson* [1969] found that the subsolar distance decreases with increasing tilt angle, but this effect is relatively weak. The increase of Ψ from $0°$ to its maximum of $35°$ results in $\Delta R_x \leq 0.03 R_x$, i.e. for $R_x = 11\ R_E$ it gives $\Delta R_x \simeq -0.3\ R_E$. Similarly, a small tilt effect at the subsolar point for $\Psi = -15°$ was predicted by *Sotirelis and Meng* [1999] (see Figure 9 in their paper), although the effect becomes more significant ($\simeq 1\ R_E$) for $\Psi = -35°$.

Thus the other models predict a weaker dipole tilt effect in the subsolar region than that predicted by the W13 model. However, only three empirical models (B00, L10 and W13) in principle are able to estimate this effect at the subsolar point. From these models, B00 was especially developed for this region and therefore may be more accurate, and its result is intermediate between two others.

Near and behind the cusps, the tilt effect predicted by both the L10 and W13 models is enhanced (while the nose B00 model does not work at high latitudes above 80°). Behind the cusps, ΔR_x changes sign, i.e. it is negative below and positive above the equatorial plane. This qualitatively agrees with the previous simulations [*Sotirelis and Meng*, 1999].

3.6. Effect of the ring current

As described in Section 2.3, we can add the RC magnetic field to the dipole field in the region outside the RC. As expected, the magnetopause distance increases in all directions (x, y, z) in the runs with the RC, because the addition of the RC is effectively equivalent to an increase of the geodipole moment and, hence, increases the magnetic field on the inner side of the magnetopause. Table 3 contains the corresponding values at the reference points in the runs of the SPBU15 with the RC corresponding to $\Delta B = -20$ nT (run SPBU-RC20) and -60 nT (SPBU-RC60).

Now let us make some simple estimates. The Earth's dipole field at the subsolar point $R_x = 11\ R_E$ is 22.7 nT. Taking into account the magnetopause currents, we should multiply this value by $f = 2.44$ [*Mead*, 1964]. According to *Shue and Chao* [2013], the coefficient f varies from ∼2.07 to 2.55, but anyway 2.44 is in this interval. Then we determine the position of the subsolar point using the pressure balance conditions for the magnetospheric magnetic pressure created only by the dipole field and the shielding magnetopause currents. This gives $R_x = 10.83\ R_E$ for the solar wind dynamic pressure of 1.338 nPa in our cases.

A symmetrical RC that produces $\Delta B = -20$ nT at the Earth provides 1.43 nT at $R_x = 11\ R_E$ (for $R_{\rm RC} = 5.5\,R_E$), i.e. 6.3% of the dipole field. We increase the Earth's magnetic moment by 6.3% and find a new magnetopause position from pressure balance at $R_x = 11.06\ R_E$ (instead of 10.83 R_E). Repeating for the moderate RC with $\Delta B = -60$ nT gives a magnetopause distance of 11.47 R_E, and for the strong RC with $\Delta B = -100$ nT gives a distance of 11.86 R_E. These estimations for the cases 0, -20, and -60 nT nearly coincide with the predictions of the new code, i.e. $R_x = 10.8$, 11.1, and 11.4 R_E. Thus we can conclude that the outward displacement of the subsolar magnetopause is $0.2-0.3$ R_E for a quiet RC with $\Delta B = -20$ nT and reaches 0.6 R_E for the RC with $\Delta B = -60$ nT.

Our estimation of the RC effect at the subsolar magnetopause seems to be smaller than that of *Schield* [1969a, b]. In that paper, a RC resulting in $\Delta B = -41$ nT at the Earth, effectively increased the Earth's dipole moment by 21% beyond 10 R_E. This enhancement of the magnetospheric magnetic field is even a little larger than that for the RC with $\Delta B = -60$ nT in our case ($R_x = 11.5\ R_E$). This difference is explained by different assumptions about the location of the RC.

Our numerical estimations agree with observations in *Hayosh et al.* [2005]. *Hayosh et al.* [2005] connected the difference between the model and observed magnetopause positions with the Dst index and found that the magnetopause moves outward on average by 0.5 R_E as Dst changes from +20 to -60 nT. This dependence of R_x on Dst is only slightly weaker than that obtained in our work. However, it should be taken into account that *Hayosh et al.* [2005] analyzed the tail region between X=-19 and X=0 R_E. Note also that the observed ground disturbance (Dst) is, roughly, a factor of 1.3 larger than the RC magnetic effect ΔB used in our study, which is quantified in the equation for the "corrected" $Dst^* = 0.8Dst - 13\sqrt{P_{dyn}}$ [e.g., *Tsyganenko and Sitnov*, 2005]. Therefore taking into account the telluric currents, the correspondence between results of Hayosh et al. (2005) and ours becomes even better.

Both R_y and R_z in the MHD simulations also increase with the RC, but R_y grows faster than R_x and R_z. As a result, the east-west elongation parameter r_{yz} increases from 1.05 for $\Delta B = 0$ to 1.07 for $\Delta B = -60$ nT.

The effect of the RC should be reproduced in SWMF-CRCM simulations. Indeed the SWMF-CRCM predicts a more distant magnetopause than the SWMF as shown in the first two columns of Table 3. In particular, R_x is larger by 0.2 R_E, R_y (R_{-y}) by 0.7 (0.6) R_E, and R_z by 0.3 R_E. Thus the CRCM makes similar or larger changes in the magnetopause distance than the RC with $\Delta B = -20$ nT in the SPBU-RC20 run, but always smaller changes than in the SPBU-RC60 run (the last predicts a difference of

0.6 R_E in R_x and 0.9 R_E in R_y as mentioned above). The calculated Dst index in the SWMF-CRCM run is 4 nT.

4. Discussion and conclusions

The magnetopause positions can be predicted using both empirical and analytical magnetopause models and global MHD models. This paper compares results from different models for the stationary typical solar wind conditions under which both empirical and MHD models should work rather well. We search for systematic differences between axisymmetric and non-axisymmetric empirical and MHD models and suggest explanations for these differences. Additionally, we find several subsolar magnetopause crossings to compare with the model predictions.

We suppose that both empirical and MHD models may have disadvantages in predicting the three-dimensional magnetopause. Empirical models make a priori assumptions about the magnetopause shape: some of them relate the radial distance to the solar zenith angle using fixed functional forms (e.g., the S98 and L10 models), while others set several fitting parameters based on implicit assumptions about most probable (rather smooth) magnetopause shape (W13). Most empirical models, except the recent L10 and W13, are axisymmetric and, hence, are inaccurate near the terminator plane. The axisymmetric models do not reproduce the cusp indentations, but also may underestimate the radial distance near the equatorial plane because of the averaging. Empirical models, again except L10 and W13, do not consider the dipole tilt angle as a control parameter. However, *Wang et al.* [2013] found that a tilt angle increase from 0° to 10° under low solar wind dynamic pressure results in a shift of the subsolar point by ∼1 R_E earthward and causes a significant deformation of the dayside magnetopause in the xz plane. In this paper, we compare the magnetopause positions in the meridional plane for tilts 15° and 0° predicted by the nose B00, L10, W13, and two MHD models and find that the all models except W13 predict a relatively small difference ΔR between $\Psi = 15°$ and 0° in the subsolar region, although ΔR increases near the cusps. We cannot decide which predictions are more accurate without additional model validation in the future.

MHD models do not include kinetic effects, but we can specify which kinetic factors are important for correct magnetopause predictions. The magnetopause position depends on the RC which is not properly described by the MHD codes. We estimate the effect of the RC at the subsolar magnetopause by modifying the SPBU15 code and making simple calculations, based on assumption of a purely dipole internal field. We find that an assumed symmetrical RC with $\Delta B = -20$ nT at the Earth and $R_{\rm RC} = 5.5\,R_E$ enhances the subsolar distance by $\simeq 0.23\ R_E$, while a stronger current with $\Delta B = -60$ nT enhances R_x by $\simeq 0.6\ R_E$. Since a strong RC ($\Delta B < -60$ nT) occurs only during magnetic storms, the correction of the subsolar distance on the RC effect in MHD results usually should not exceed $0.5\ R_E$. However, this estimate depends on the radius of the RC. A symmetrical RC located farther from the Earth results in a stronger effect at the subsolar magnetopause. Moreover, the shape of the ring current in the dayside magnetosphere is still not well established and may differ from a torus [*Kirpichev and Antonova*, 2014; *Andreeva and Tsyganenko*, 2016] which would also influence the magnetopause position.

Global MHD models coupled with the inner magnetospheric models, e.g., with the RCM or CRCM, may better reproduce the location of the magnetopause. In particular, the results of the SWMF-CRCM in the $Bz0$ case approach the results of the empirical L10 model closer than the results of SWMF without the ring current model. However, the difference between the SWMF and SWMF-CRCM at the subsolar magnetopause is only 0.2 R_E while *Pembroke et al.* [2012] reported that the magnetopause lies about 1 R_E sunward in the coupled LFM-RCM run than in the uncoupled LFM run.

The magnetopause current is calculated from the curl of the magnetic field and should in general be correctly reproduced in MHD simulations as well as the magnetic field itself. However, the accuracy of magnetospheric-ionospheric currents may significantly depend on specifics of a particular MHD code [*Gordeev et al.*, 2015]. We believe that these currents in the dayside magnetosphere are stronger and exert more influence on the magnetopause position in the $Bz-$ case, rather than in the $Bz0$ and $Bz+$ cases. The cross-tail current should be reasonably well reproduced by MHD models, and its effect at the subsolar magnetopause is relatively small [*Schield*, 1969a; *Tsyganenko and Sibeck*, 1994].

We can suggest several other reasons why MHD codes may inaccurately predict magnetopause positions. First, kinetic processes may cause the solar wind dynamic pressure to significantly decrease in the foreshock region upstream of the bow shock [*Fairfield et al.*, 1990].

For a nearly radial IMF the total pressure near the magnetopause occasionally drops up to 20 % of the solar wind pressure [*Suvorova et al.*, 2010]. However, such significant changes occur for nearly radial IMF conditions which rarely occur in the solar wind (although the radial IMF events were observed more often than usually in 2007-2008). In the cases studied here, the cone angle between the IMF and x axis is equal to or larger than 45°. Although the IMF is not radial, we suppose that the solar wind dynamic pressure immediately upstream of the bow shock may differ from the pressure observed by a solar wind monitor near the L1 point. This effect is not well studied in observations, because the plasma parameters from the solar wind monitors near the L1 point and close to the bow shock (e.g., from ACE and THEMIS) are often intercalibrated, which eliminates differences between them.

Samsonov et al. [2012] showed that the total pressure varies along the Sun-Earth line across the magnetosheath and these variations depend on the IMF orientation. *Shue and Chao* [2013] expressed the magnetopause pressure balance in the form $(fB_e/R_x^3)^2 \sim kP_{dyn}$, where B_e is the magnetic field strength on the equatorial surface of the Earth, f is the coefficient reflecting the role of magnetopause currents, and the coefficient k denotes the fraction of the solar wind dynamic pressure applied to the magnetopause. *Shue and Chao* [2013] showed that f can vary from ∼2.07 to 2.55, and k can vary from 0.74 to 0.94, depending on the IMF B_z and solar wind dynamic pressure. MHD models self-consistently take into account both the changes of the total pressure across the magnetosheath and the magnetopause deformation (since f varies depending on the magnetopause shape and electric current). Empirical models are based on measured upstream parameters and observed magnetopause locations, consequently, both f and k variations are included but they cannot be separated.

MHD models predict the thermal pressure in the dayside outer magnetosphere $p \simeq 0.1$ nPa which is in general agreement with quiet-time observations [e.g., *Phan et al.*, 1994; *Shue and Chao*, 2013]. Simulations using an anisotropic MHD model (anisotropic MHD equations for the local magnetosheath model presented by *Samsonov et al.* [2007]) (not shown) indicate that anisotropic pressures only slightly change the subsolar magnetopause distance. This agrees with global anisotropic MHD results of the uncoupled BATS-R-US (later developed to SWMF) code [*Meng et al.*, 2013], while the subsolar point predicted by the anisotropic BATS-R-US coupled with both RCM or CRCM is ∼0.4-0.5 R_E closer to the Earth than that predicted by the corresponding isotropic code.

Comparing predictions of empirical and MHD models, we emphasize several items.

Positions of the subsolar point in the $Bz0$ case.

The average distance to the subsolar point from all axisymmetric empirical models (PR96, KS98, P98, S98) is 11.1 R_E, which agrees with both the average subsolar position obtained for seven selected events (11.2 R_E) and R_x predicted by the SWMF and the SPBU-R20 code (with the added symmetrical RC with $\Delta B = -20$ nT and $R_{\rm RC} = 5.5\, R_E$). Other MHD codes, LFM and OpenGGCM, predict a smaller distance $R_x = 10.4$ R_E. The difference between MHD predictions may be explained by different boundary conditions at the low-altitude boundary, affecting the plasma pressure inside the magnetopause.

The two global non-axisymmetric empirical models (L10 and W13) predict $R_x = 11.47$, and 12.60 R_E respectively, i.e., larger than both axisymmetric empirical and MHD models. To check this prediction, we have additionally calculated R_x using the local (for the nose region) empirical model of *Boardsen et al.* [2000] and obtained 11.84 R_E, i.e. between the L10 and W13 results. As discussed above, the axisymmetric empirical models (e.g., PR96 or S98) do not take into account the dipole tilt effect and therefore may underestimate the subsolar distance for zero tilt. In the selected events, the average tilt angle is $|\Psi| = 5.3°$, i.e., the average R_x may still differ from that in the untilted case $\Psi = 0°$. In event with Ψ closest to zero, we get the largest $R_x^{cor} \simeq 11.68$. MHD models may underestimate the subsolar distance for several reasons, such as the RC effect or depressed solar wind dynamic pressure upstream of the bow shock.

Since R_x predicted by empirical and MHD models for the same conditions scatters from 10.4 to 12.6 R_E, it is difficult to determine just one most probable distance. However, consistent with the arguments above, we believe that the actual subsolar distance in the $Bz0$ case for $\Psi = 0°$ is located between 11.0 and 12.0 R_E, i.e. in the interval which includes R_x from two MHD models with the ring current magnetic field (SWMF-CRCM, SPBU-RC) and from two of three non-axisymmetric empirical models (B00, L10) as well as consistent with THEMIS observations used in our study. Since only one non-axisymmetric model (W13) predicts $R_x > 12$ R_E, we cannot rely on this prediction without future verification.

Dawn–dusk elongation and positions of reference points in the terminator plane.

Calculations for the *Mead and Beard* [1964] magnetopause model based on the pressure balance between the dipole field and solar wind pressure give $r_{yz} = R_y/R_z \simeq 1.22$. In our $Bz0$ case, the asymmetric empirical models, L10 and W13, predict respectively $r_{yz} \simeq 1.12$ and 1.19, while the MHD SWMF and LFM give 1.11 and 1.10. The difference between the predictions of the L10 and W13 models is not in R_z, but in R_y, therefore it is related to a larger radial distance to the magnetopause near the equatorial plane for $\Psi = 0°$ in the W13 model. The MHD models may underestimate r_{yz} because of the absence of the RC contribution to the magnetic field.

In the $Bz+$ case, r_{yz} increases to 1.23 in the W13 model, and to 1.14 and 1.11 in SWMF and LFM, respectively. This increase is mainly caused by a R_z decrease which can be explained by the enhanced magnetic reconnection behind the cusps for northward IMF. Consequently, in the $Bz-$ case, the r_{yz} decreases to 1.14 in the W13 model, to 1.04 and

0.93 in the SWMF and LFM models respectively. The L10 model predicts insignificant changes in r_{yz} for the $Bz+$ and $Bz-$ cases. Thus only one empirical model (W13) may in principle correctly predict the dawn–dusk elongation and its variations with the B_z sign, and the MHD model predictions differ from each other.

Comparing predictions of MHD models with the ring current (SWMF-CRCM, SPBU-RC20, and SPBU-RC60) and non-axisymmetic empirical models (L10, W13, and SG15 for R_z) for reference points in the terminator plane, we get a relatively good agreement between them. In particular, R_z in the case $Bz0$ is between 14.6 and 15.6 R_E as confirmed by all these models. The range of R_y predicted by SWMF-CRCM, SPBU-RC and L10 is from 15.9 to 16.4 R_E, while W13 yields 17.9 R_E. The magnitude R_{-y} is about 0.5 R_E larger than R_y.

Comparison between northward and southward IMF cases.

The difference between the $Bz+$ and $Bz-$ cases is evaluated by means of the parameter $\Delta R_x = R_x(Bz+) - R_x(Bz-)$. Its value varies from 0.28 R_E in the S98 model to 0.89 and 0.95 in the W13 and P98 models. The MHD models predict ΔR_x within a narrower (or the same) range of values, e.g., 0.1 R_E in SWMF and 0.6 R_E in LFM. In the MHD codes, the ΔR_x probably depends on the magnitude of magnetospheric-ionospheric currents.

As mentioned above, R_z decreases from southward to northward IMF, however only the W13 and SG15 empirical models predict such a decrease, with $\Delta R_z = -1.16$ and -0.50 R_E respectively. All MHD models predict negative ΔR_z, e.g., -1.3 R_E in SWMF and -2.5 R_E in LFM, and $|\Delta R_z|$ is larger than in the empirical models. The ΔR_y is relatively small both in empirical and in MHD models.

A slightly larger compression on the dusk flank due to the Parker spiral IMF.

When the IMF is oriented along the Parker spiral, the dusk magnetosphere lies downstream of the quasi-perpendicular bow shock, and the dawn magnetosphere lies downstream of the quasi-parallel bow shock. Since the magnetosheath magnetic field is larger downstream from the quasi-perpendicular bow shock, the total pressure on the duskside magnetopause is higher than that on the dawnside magnetopause. Consequently the magnetopause distance is smaller on the dusk side than on the dawn side. Among the empirical models, only L10 is able to reproduce this effect. W13 model uses only the dynamic pressure and B_z in the solar wind data and therefore assumes symmetry across the noon-meridional plane. On the contrary, all MHD models, except LFM, predict this difference. LFM model does not predict this effect because of the fixed solar wind condition $B_x = 0$ used in the runs presented here. The L10 model predicts $R_y + R_{-y} = -0.5$ R_E, very similar to the predictions of the SWMF and SPBU15 codes.

Differences between the empirical and MHD models.

Axisymmetric empirical magnetopause models do not reproduce the three-dimensional magnetopause and lose information due to the tilt angle averaging. The position of the subsolar point in the axisymmetric models (PR96, S98) is closer to the Earth than in the non-axisymmetric models (B00, L10, W13) for $\Psi = 0°$. In general, all the reference points (R_x, R_y, R_z) predicted by the non-axisymmetric models are also farther from the Earth than the corresponding points predicted by the numerical models (SWMF, LFM) in the $Bz0$ and $Bz+$ cases, i.e., the MHD codes most likely underestimate the magnetopause distance. However, predictions of the SPBU15 code with the relatively strong RC with

$\Delta B = -60$ nT (SPBU-RC60) are close to the L10 results in R_x, R_y and R_{-y} in the $Bz0$ case, while R_z in the MHD results on 0.5 R_E larger than in L10, but nearly equal to the prediction of the SG15 empirical model developed for the high-latitude magnetopause. The magnetopause position predicted by the SWMF coupled with the CRCM is closer to the L10 model than that in the uncoupled SWMF, but the magnetopause distance in the SWMF-CRCM run is still slightly underestimated in comparison with L10.

Summarizing the large amount of information in this paper, we still cannot give a positive answer to the question in the title. Comparing MHD models in which the ring current magnetic field is taken into account (BATSRUS-CRCM, SPBU-RC) with the empirical non-axisymmetric L10 model, we find that the differences in the reference point positions predicted by these models are relatively small. Therefore we assume that these predictions indicate the actual magnetopause position in the Bz0 case. However, the large difference between L10 and W13 results (> 1 R_E) near the equatorial plane requires further investigation. In some respects, the W13 model makes more reasonable predictions, e.g. when it successfully reproduces the effect of a southward IMF at the terminator plane. It is also important to note that W13 employs the largest database, including crossings from both recent and old missions, because some missions (THEMIS, MMS) have an apogee in the subsolar region near 12 R_E and may miss more distant magnetopause crossings. We believe that the role of the dipole tilt on the magnetopause position is still not completely understood. Furthermore, the next generation of magnetopause models should treat magnetopause crossings for nearly radial IMF separately, because these are times when the magnetosheath pressure becomes significantly lower than the solar wind dynamic pressure [*Suvorova and Dmitriev*, 2015]. If the number of such events in a magnetopause crossings database is relatively large, the models which do not consider the IMF cone angle as an input parameter will overestimate the magnetopause distance. Finally, we hope that the results of our work can help to develop a new three-dimensional empirical magnetopause model which can give a positive answer to the question in the title.

Acknowledgments. This work was supported by the Russian Foundation for Basic Research grant 14-05-00399. The work by E.G. was supported by RFBR grant 14-05-31380. J. Šafránková and Z. Němeček thank to the Czech Grant Agency for support under Contract 14-19376S. AAS thanks Prof. Victor Sergeev for valuable comments. We thank Dr. Yongli Wang for providing results of the W13 model. Simulation results were provided by the Community Coordinated Modeling Center (http://ccmc.gsfc.nasa.gov) at Goddard Space Flight Center. THEMIS data are available from the Coordinated Data Analysis Web (CDAWeb) and THEMIS web site (http://themis.igpp.ucla.edu). OMNI data are available from OMNIWeb service (http://omniweb.gsfc.nasa.gov).

References

Andreeva, V. A., and N. A. Tsyganenko (2016), Reconstructing the magnetosphere from data using radial basis functions, *J. Geophys. Res. Space Physics*, *121*, 2249–2263, doi: 10.1002/2015JA022242.

Beard, D. B. (1960), The interaction of the terrestrial magnetic field with the solar corpuscular radiation, *J. Geophys. Res.*, *65(11)*, 3559-3568, doi:10.1029/JZ065i011p03559.

Boardsen, S. A., T. E. Eastman, T. Sotirelis, and J. L. Green (2000), An empirical model of the high-latitude magnetopause, *J. Geophys. Res.*, *105(A10)*, 23,193–23,219, doi:10.1029/1998JA000143.

Brackbill J. U. and D. C. Barnes (1980), The effect of nonzero $\nabla \cdot \mathbf{B}$ on the numerical solution of the magnetohydrodynamic equations, *J. Comput. Phys. 35*, 426–430, doi: 10.1016/0021-9991(80)90079-0.

Chapman, S., and V. C. A. Ferraro (1931), A new theory of magnetic storms, *Terr. Magn. Atmos. Electr.*, *36(2)*, 77–97, doi:10.1029/TE036i002p00077.

De Zeeuw, D., S. Sazykin, R. Wolf, T. Gombosi, A. Ridley, and G. Toth (2004), Coupling of a global MHD code and an inner magnetosphere model: Initial results, *J. Geophys. Res.*, *109(A12)*, A12219, doi:10.1029/2003JA010366.

Dmitriev, A. V., and A. V. Suvorova (2000), Three-dimensional artificial neural network model of the dayside magnetopause, *J. Geophys. Res.*, *105*, 18,909-18,918, doi: 10.1029/2000JA900008.

Dungey J. W. (1961), Interplanetary magnetic field and the auroral zones, *Phys. Rev. Lett.* *6*, 47–48.

Elsen, R. K., and R. M. Winglee (1997), The average shape of the Magnetopause: A comparison of three-dimensional global MHD and empirical models, *J. Geophys. Res.*, *102(A3)*, 4799-4819, doi:10.1029/96JA03518.

Fairfield, D. H. (1971), Average and unusual locations of the Earth's magnetopause and bow shock, *J. Geophys. Res.*, *76(28)*, 6700-6716, doi:10.1029/JA076i028p06700.

Fairfield, D. H., Baumjohann, W., Paschmann, G., Lühr, H., Sibeck, D. G. (1990), Upstream pressure variations associated with the bow shock and their effects on the magnetosphere, *J. Geophys. Res.*, *95(A4)*, 3773–3786, doi:10.1029/JA095iA04p03773.

Fok, M., R. A. Wolf, R. W. Spiro, and T. E. Moore (2001), Comprehensive computational model of Earth's ring current, *J. Geophys. Res.*, *106*, 8417-8424, doi: 10.1029/2000JA000235.

García, K. S., and W. J. Hughes (2007), Finding the Lyon-Fedder-Mobarry magnetopause: A statistical perspective, *J. Geophys. Res.*, *112*, A06229, doi:10.1029/2006JA012039.

Glocer, A., M. Fok, X. Meng, G. Tóth, N. Buzulukova, S. Chen, and K. Lin (2013), CRCM + BATS-R-US two-way coupling, *J. Geophys. Res.*, *118*, 1635-1650, doi: 10.1002/jgra.50221.

Gombosi, T. I., G. Tóth, D. L. De Zeeuw, K. C. Hansen, K. Kabin, K. G. Powell (2002), Semirelativistic magnetohydrodynamics and physics-based convergence acceleration, *J. Comput. Phys.*, *177,* 176-205, doi:10.1006/jcph.2002.7009.

Gordeev, E., V. Sergeev, I. Honkonen, M. Kuznetsova, L. Rastätter, M. Palmroth, P. Janhunen, G. Tóth, J. Lyon, and M. Wiltberger (2015), Assessing the performance of community-available global MHD models using key system parameters and empirical relationships, *Space Weather*, *13*, doi:10.1002/2015SW001307.

Hayosh, M., Z. Němeček, J. Šafránková, and G. N. Zastenker (2005), Variations of the magnetosheath ion flux and geomagnetic activity, *Adv. Space Res.*, *36(12)*, 2417-2422, doi:10.1016/j.asr.2003.08.082.

Hellinger, P., P. Travnicek, J. C. Kasper, and A. J. Lazarus (2006), Solar wind proton temperature anisotropy: Linear theory and WIND/SWE observations, *Geophys. Res. Lett.*, *33*, L09101, doi:10.1029/2006GL025925.

Hill, T. W., and M. E. Rassbach (1975), Interplanetary magnetic field direction and the configuration of the day side magnetosphere, *J. Geophys. Res.*, *80(1)*, 1-6, doi: 10.1029/JA080i001p00001.

Kirpichev, I. P., and E. E. Antonova (2014), Estimation of the Current Density and Analysis of the Geometry of the Current System Surrounding the Earth, *Cosmic Research 52*, 52–60, doi:10.1134/S0010952514010043.

Kovner, M. S., and Y. I. Feldstein (1973), On solar wind interaction with the earth's magnetosphere, *Planet. Space Sci. 21*, 1191–1211, doi:10.1016/0032-0633(73)90206-7.

Kuznetsov, S. N., and A. V. Suvorova (1998), An empirical model of the magnetopause for broad ranges of solar wind pressure and Bz IMF, in *Polar Cap Boundary Phenomena*, edited by J. Moen, A. Egeland, and M. Lockwood, pp. 51-61, Kluwer Acad., Norwell, Mass.

Lin, R. L., X. X. Zhang, S. Q. Liu, Y. L. Wang, and J. C. Gong (2010), A three-dimensional asymmetric magnetopause model, *J. Geophys. Res.*, *115*, A04207, doi:10.1029/2009JA014235.

Lu, J. Y., Z.-Q. Liu, K. Kabin, M. X. Zhao, D. D. Liu, Q. Zhou, and Y. Xiao (2011), Three dimensional shape of the magnetopause: Global MHD results, *J. Geophys. Res.*, *116*, A09237, doi:10.1029/2010JA016418.

Lyon, J. G., J. A. Fedder, and C. M. Mobarry (2004), The Lyon-Fedder-Mobarry (LFM) global MHD magnetospheric simulation code, *J. Atmos. Sol.-Terr. Phys.*, *66*, 1333–1350, doi:10.1016/j.jastp.2004.03.020.

Maltsev, Y. P., and W. B. Lyatsky (1975), Field aligned currents and erosion of the dayside magnetosphere, *Planet. Space Sci.*, *23*, 1257-1260, doi:10.1016/0032-0633(75)90149-X.

Mead, G. D. (1964), Deformation of the geomagnetic field by the solar wind, *J. Geophys. Res.*, *69*(7), 1181-1195, doi:10.1029/JZ069i007p01181.

Mead, G. D., and D. B. Beard (1964), Shape of the geomagnetic field solar wind boundary, *J. Geophys. Res.*, *69(7)*, 1169-1179, doi:10.1029/JZ069i007p01169.

Meng, X., G. Tóth, A. Glocer, M.-C. Fok, and T. I. Gombosi (2013), Pressure anisotropy in global magnetospheric simulations: Coupling with ring current models, *J. Geophys. Res.*, *118*, 5639-5658, doi:10.1002/jgra.50539.

Merkin, V. G., and J. G. Lyon (2010), Effects of the low-latitude inospheric boundary condition on the global magnetosphere, *J. Geophys. Res.*, *115*, doi:10.1029/2010JA015461.

Merkin, V. G., Lyon, J. G., and Claudepierre, S. G. (2013), Kelvin-Helmholtz instability of the magnetospheric boundary in a three-dimensional global MHD simulation during northward IMF conditions, *J. Geophys. Res.*, *118*, 5478-5496. doi:10.1002/jgra.50520.

Němeček, Z., J. Šafránková, O. Kruparova, L. Přech, K. Jelínek, Š. Dušík, J. Šimunek, K. Grygorov, and J.-H. Shue (2015), Analysis of temperature versus density plots and their relation to the LLBL formation under southward and northward IMF orientations, *J. Geophys. Res. Space Physics*, *120*, 3475-3488, doi:10.1002/2014JA020308.

Olson, W. P. (1969), The shape of the tilted magnetopause, *J. Geophys. Res.*, *74(24)*, 5642-5651, doi:10.1029/JA074i024p05642.

Palmroth, M., T. I. Pulkkinen, P. Janhunen, and C.-C. Wu (2003), Stormtime energy transfer in global MHD simulation, *J. Geophys. Res.*, *108(A1)*, 1048, doi: 10.1029/2002JA009446.

Pembroke, A., F. Toffoletto, S. Sazykin, M. Wiltberger, J. Lyon, V. Merkin, and P. Schmitt (2012), Initial results from a dynamic coupled magnetosphere-ionosphere-ring current model, *J. Geophys. Res.*, *117*, A02211, doi:10.1029/2011JA016979.

Petrinec, S. P., P. Song, and C. T. Russell (1991), Solar cycle variations in the size and shape of the magnetopause, *J. Geophys. Res.*, *96(A5)*, 7893-7896, doi:

10.1029/90JA02566.

Petrinec, S. M., and C. T. Russell (1993), External and internal influences on the size of the dayside terrestrial magnetosphere, *Geophys. Res. Lett.*, *20*, 339–342, doi: 10.1029/93GL00085.

Petrinec, S. M., and C. T. Russell (1996), Near-Earth magnetotail shape and size as determined from the magnetopause flaring angle, *J. Geophys. Res.*, *101*, 137-152, doi: 10.1029/95JA02834.

Phan, T.-D., G. Paschmann, W. Baumjohann, N. Sckopke, and H. Lühr (1994), The magnetosheath region adjacent to the dayside magnetopause: AMPTE/IRM observations, *J. Geophys. Res.*, *99(A1)*, 121-141, doi:10.1029/93JA02444.

Pudovkin, M. I., N. A. Tsyganenko, and A. V. Usmanov (1986), The influence of longitudinal currents on the magnetopause on the structure and position of polar cusps, *Geomagn. Aeron.*, Engl. Transl., *26*, 801–805.

Pudovkin, M. I., B. P. Besser, and S. A. Zaitseva (1998), Magnetopause stand-off distance in dependence on the magnetosheath and solar wind parameters, *Ann. Geophys.*, *16*, 388–396.

Raeder, J., et al. (2001), Global simulation of the Geospace Environment Modeling substorm challenge event, *J. Geophys. Res.*, *106*, 381–395, doi:10.1029/2000JA000605.

Samsonov, A. A., O. Alexandrova, C. Lacombe, M. Maksimovic, and S. P. Gary (2007), Proton temperature anisotropy in the magnetosheath: comparison of 3-D MHD modelling with Cluster data, *Ann. Geophys.*, *25*, 1157–1173, doi:10.5194/angeo-25-1157-2007.

Samsonov, A. A., Z. Němeček, J. Šafránková, and K. Jelínek (2012), Why does the subsolar magnetopause move sunward for radial interplanetary magnetic field?, *J. Geophys. Res.*, *117*, A05221, doi:10.1029/2011JA017429.

Schield, M. A. (1969a), Pressure balance between solar wind and magnetosphere, *J. Geophys. Res.*, *74(5)*, 1275-1286, doi:10.1029/JA074i005p01275.

Schield, M. A. (1969b), Correction to paper by Milo A. Schield, Pressure balance between solar wind and magnetosphere, *J. Geophys. Res.*, *74(21)*, 5189-5190, doi: 10.1029/JA074i021p05189.

Shue, J.-H., et al. (1998), Magnetopause location under extreme solar wind conditions, *J. Geophys. Res.*, *103*, 17,691–17,700, doi:10.1029/98JA01103.

Shue, J.-H., and J.-K. Chao (2013), The role of enhanced thermal pressure in the earthward motion of the Earth's magnetopause, *J. Geophys. Res.*, *118*, 3017-3026, doi: 10.1002/jgra.50290.

Shukhtina, M. A., and E. Gordeev (2015), In situ magnetotail magnetic flux calculation, *Ann. Geophys.*, *33*, 769–781, doi:10.5194/angeo-33-769-2015.

Sibeck, D. G., R. E. Lopez, and E. C. Roelof (1991), Solar wind control of the magnetopause shape, location, and motion, *J. Geophys. Res.*, *96(A4)*, 5489-5495, doi: 10.1029/90JA02464.

Sotirelis, T., and C.-I. Meng (1999), Magnetopause from pressure balance, *J. Geophys. Res.*, *104(A4)*, 6889-6898, doi:10.1029/1998JA900119.

Spreiter, J. R., and B. R. Briggs (1962), Theoretical determination of the form of the boundary of the solar corpuscular stream produced by interaction with the magnetic dipole field of the Earth, *J. Geophys. Res.*, *67(1)*, 37-51, doi:10.1029/JZ067i001p00037.

Spreiter, J. R., A. L. Summers, and A. Y. Alksne (1966), Hydromagnetic flow around the magnetosphere, *Planet. Space Sci.*, *14*, 223–253, doi:10.1016/0032-0633(66)90124-3.

Suvorova, A. V., and A. V. Dmitriev (2015), Magnetopause inflation under radial IMF: Comparison of models, *Earth and Space Science*, *2*, 107-114, doi: 10.1002/2014EA000084.

Suvorova, A. V., et al. (2010), Magnetopause expansions for quasi-radial interplanetary magnetic field: THEMIS and Geotail observations, *J. Geophys. Res.,* *115*, A10,216, doi:10.1029/2010JA015404.

Tanaka T. (1994), Finite volume TVD scheme on an unstructured grid system for three-dimensional MHD simulations of inhomogeneous systems including strong background potential field, *J. Comp. Phys.*, *111*, 381–389, doi:10.1006/jcph.1994.1071.

Toffoletto, F. R., S. Sazykin, R. W. Spiro and R. A. Wolf (2003), Modeling the Inner Magnetosphere using the Rice Convection Model (review), *Space Sci. Rev.*, *108*, 175–196.

Tóth, G., et al. (2005), Space Weather Modeling Framework: A new tool for the space science community, *J. Geophys. Res.*, *110*, A12226, doi:10.1029/2005JA011126.

Tóth, G., et al. (2012), Adaptive Numerical Algorithms in Space Weather Modeling, *Journal of Computational Physics*, *231*, 870, doi:10.1016/j.jcp.2011.02.006.

Tsyganenko, N. A., and D. G. Sibeck (1994), Concerning flux erosion from the dayside magnetosphere, *J. Geophys. Res.*, *99(A7)*, 13425-13436, doi:10.1029/94JA00719.

Tsyganenko, N. A. (1995), Modeling the Earth's magnetospheric magnetic field confined within a realistic magnetopause, textitJ. Geophys. Res., *100(A4)*, 5599-5612, doi: 10.1029/94JA03193.

Tsyganenko, N. A. (1996), Effects of the solar wind conditions on the global magnetospheric configuration as deduced from data-based field models, in *European Space Agency Publication, ESA SP, 389*, 181-185.

Tsyganenko, N. A., and M. I. Sitnov (2005), Modeling the dynamics of the inner magnetosphere during strong geomagnetic storms, *J. Geophys. Res.*, *110*, doi: 10.1029/2004JA010798.

Tsyganenko, N. A., and V. A. Andreeva (2015), A forecasting model of the magnetosphere driven by an optimal solar wind coupling function, *J. Geophys. Res.*, *120*, doi: 10.1002/2015JA021641.

Wang, Y., D. G. Sibeck, J. Merka, S. A. Boardsen, H. Karimabadi, T. B. Sipes, J. Šafránková, K. Jelínek, and R. Lin (2013), A new three-dimensional magnetopause model with a support vector regression machine and a large database of multiple spacecraft observations, *J. Geophys. Res.*, *118*, 2173-2184, doi:10.1002/jgra.50226.

Wolf, R. A., R. W. Spiro, and F. J. Rich (1991), Extension of the Rice Convection Model into the high-latitude ionosphere, *J. Atm. Terrest. Phys.*, *53*, 817–829.

Xi, S., W. Lotko, B. Zhang, O. J. Brambles, J. G. Lyon, V. G. Merkin, and M. Wiltberger (2015), Poynting flux-conserving low-altitude boundary conditions for global magnetospheric models, *J. Geophys. Res. Space Physics*, *120*, 384-400, doi: 10.1002/2014JA020470.

Zhigulev, V. N., and E. A. Romishevskii (1959), Concerning the interaction of currents flowing in a conducting medium with the earth's magnetic field, *Soviet Phys. Doklady*, *5*, 1001–1004 (Eng. Trans. 1960, *4*, 859–862).

Table 1. List of empirical (analytical) magnetopause models

Model	PR96	KS98	P98	S98	B00	L10	W13	SG15
non-axisymmetric	N	N	1 point	N	Y	Y	Y	1 point
dipole tilt	N	N	N	N	Y	Y	Y	Y
analytical form	Y	Y	Y	Y	Y	Y	N	Y
number of crossings	6273	886	Analit.(33)	553	290	2708	15,089	1022

[a] Abbreviations of models: PR96 [*Petrinec and Russell*, 1996], KS98 [*Kuznetsov and Suvorova*, 1998], P98 [*Pudovkin et al.*, 1998], S98 [*Shue et al.*, 1998], B00 [*Boardsen et al.*, 2000], L10 [*Lin et al.*, 2010], W13 [*Wang et al.*, 2013], SG15 [*Shukhtina and Gordeev*, 2015].

Table 2. Results from the empirical (analytical) magnetopause models in the case $Bz0$ ($N = 5$ cm^{-3}, $V_x = -400$ km/s, $T = 2 \times 10^5$ K, $B_y = -B_x = 3.5$ nT and $B_z = 0$).

Model	PR96	KS98	P98	S98	B00	L10	W13	SG15
R_x	11.10	11.45	10.99	10.90	11.84	11.47	12.60	
R_y	15.78	16.52		16.33		16.44	17.90	
R_{-y}						-16.94		
R_z						15.00	15.00	15.66
R_{-z}						-14.91		

[a] R_x is the magnetopause intersections with the x axis, R_y and R_z are the intersections with the y and z axes, R_{-y} and R_{-z} are the intersections with -y and -z. All values are given in R_E.

Table 3. Results from the MHD models in the run $Bz0$.

Model	SWMF	SWMF-CRCM	LFM	GGCM	SPBU	SPBU-RC20	SPBU-RC60
R_x	11.1	11.3	10.4	10.4	10.8	11.1	11.4
R_y	15.7	16.4	15.5	13.2	15.5	15.9	16.4
R_{-y}	-16.1	-16.7	-15.5	-14.0	-16.0	-16.4	-16.9
R_z	14.3	14.6	14.1	16.5	15.0	15.2	15.5

[a] The abbreviations 'SPBU-RC20' and 'SPBU-RC60' denote the results of the SPBU15 for the ring current yielding $\Delta B = -20$ and -60 nT at the Earth.

Table 4. Magnetopause crossings in the subsolar region observed by THEMIS

Date	Time	SC	*Robs*	x, y, z(GSM)	R_x^{cor}	P_{dyn},nPa	B_z,nT	Ψ	Dst
30.09.2009	16:46	THE	<11.02	10.9, -1.6, -0.2	10.80/11.67	1.2/2.0	5.5	7.0	2
11.10.2009	20:01	THD	>11.42	11.4, -0.5, 0.9	11.88/11.49	1.7/1.4	-0.5	-1.0	-5
25.10.2009	13:05	THA	<11.68	11.5, -0.9, 1.6	10.96/11.72	0.9/1.4	-1.1	-6.0	-17
02.11.2009	18:52	THD	≃11.37	10.4, -4.1, 1.9	≃10.92	1.2	1.2	-6.7	1
19.10.2010	20:03	THA	≃11.57	11.0, 2.4, 2.5	11.67/11.24	1.5/1.2	4.3	-4.0	-13
03.11.2010	16:33	THE	>11.38	10.9, -1.4, 2.9	>11.27	1.4	0.6	-5.2	-16
08.02.2015	14:52	THD	>10.37	10.1, -2.1, 1.4	>10.57	1.6	4.8	-7.0	-20

[a] THA, THD, and THE denote THEMIS A, D, and E. *Robs* is the observed radial distance, R_x^{cor} is the corrected subsolar distance calculated for $P_{dyn} = 1.34$ nPa. Ψ is the dipole tilt angle (in degrees), Dst index in nT.

Table 5. The differences between magnetopause positions in the northward and southward cases ($R(Bz+) - R(Bz-)$) in the empirical models.

Model	PR96	KS98	P98	S98	B00	L10	W13	SG15	Aver.
ΔR_x	0.51	0.53	0.95	0.28	0.23	0.57	0.89		0.57*
ΔR_y	0.0	0.57		-0.05		0.38	-0.15		
ΔR_z						0.38	-1.16	-0.50	

* The last column contains the average ΔR_x for six models.

Table 6. The differences ($R(Bz+) - R(Bz-)$) in the MHD simulations.

Model	SWMF	LFM	GGCM	SPBU	Aver.
ΔR_x	0.1	0.6	0.7	0.2	0.4
ΔR_y	0.2	0.2	1.6	0.8	0.4*
ΔR_z	-1.3	-2.5	-2.7	-0.7	-1.5*

* The last column contains the average ΔR_y and ΔR_z for all models, except GGCM.

Figure 1. Electric current density obtained by the SWMF in the run $Bz0$ in the equatorial ($z = 0$), noon-meridional ($y = 0$) and terminator ($x = 0$) planes. Thick white lines indicate the boundary between open and closed magnetic field lines determined by magnetic field line tracing. This boundary partly coincides with the maximum of electric current. We use the following solar wind conditions: $N = 5$ cm^{-3}, V_x=-400 km/s, $T = 2 \times 10^5$ K, $B_y = -B_x = 3.5$ nT and $B_z = 0$. The units in color bar are nA/m^2.

Figure 2. Magnetopause positions in the equatorial and noon-meridional planes obtained by empirical and numerical MHD models: black solid [*Shue et al.*, 1998], black dashed [*Wang et al.*, 2013], blue (SWMF), green (LFM), and red lines (SPBU15 without the ring current). The solar wind conditions are the same as those in Figure 1.

Figure 8. Magnetopause positions in the noon-meridional plane in the northward (solid) and southward (dashed) IMF cases. Panel a: black [*Shue et al.*, 1998], blue [*Wang et al.*, 2013]; panel b: blue (SWMF), green (LFM), and red lines (SPBU15). Solar wind conditions are the following: $N = 5$ cm^{-3}, V_x=-400 km/s, $T = 2 \times 10^5$ K, $B_y = -B_x = 3.5$ nT and $B_z = \pm 3$ nT.

Figure 4. Differences between the distances to the magnetopause for tilted and non-tilted dipoles ($\Delta R = R(\Psi = 15°) - R(\Psi = 0°)$) in the noon-meridional plane as a function of the latitude $\theta = \arctan(z/x)$. Solid black line corresponds to the W13 model, dashed black line to the B00 model, red line to the L10 model, and blue line to the SWMF.

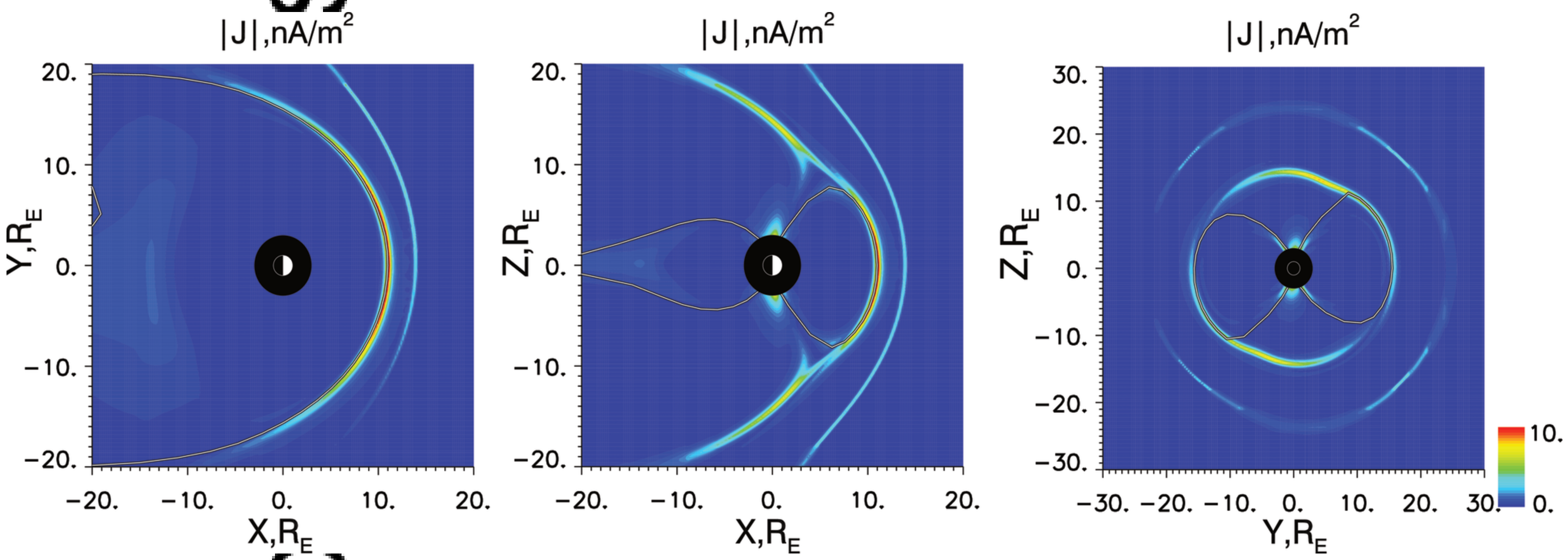

2016ja022471-f01-z-.eps

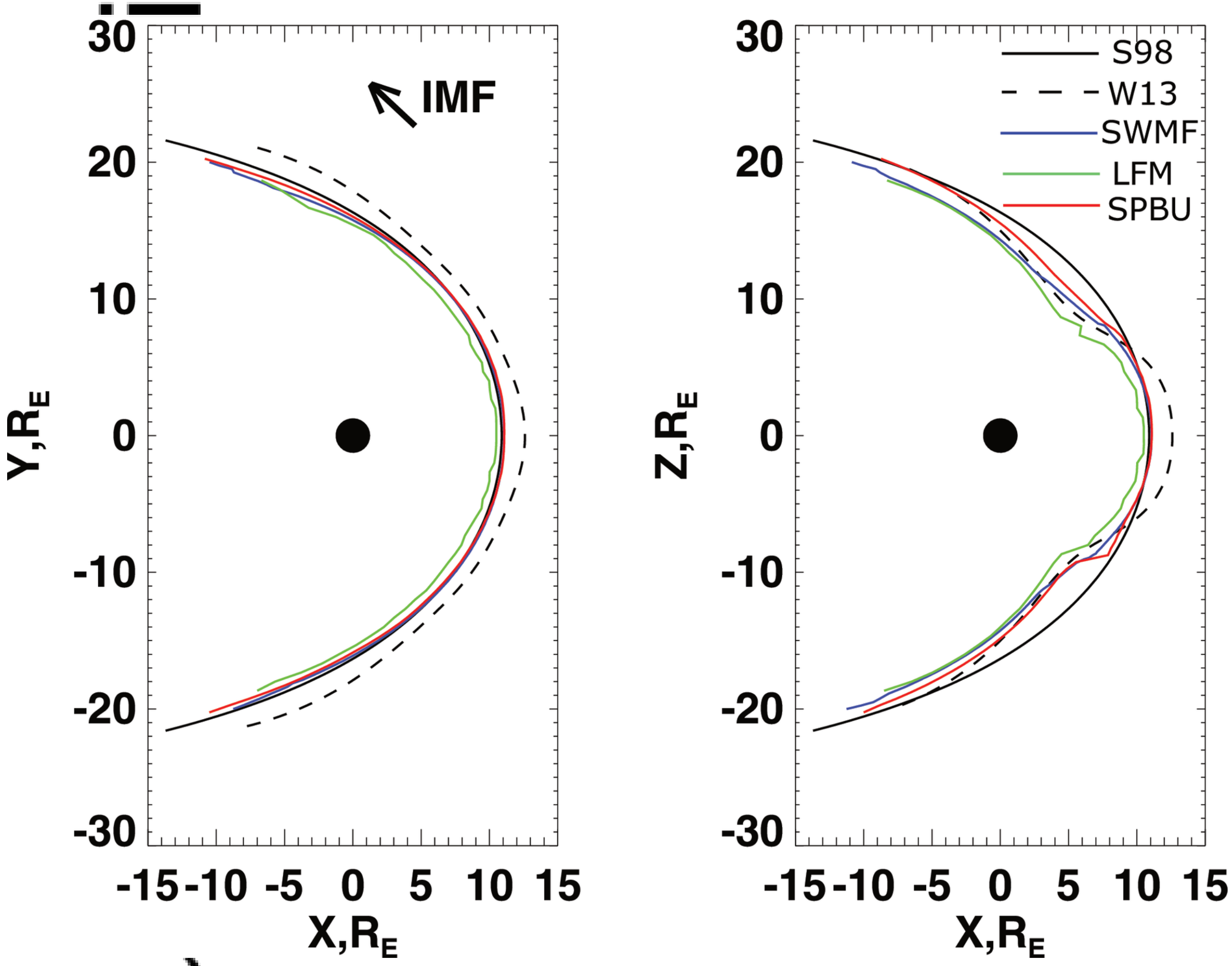

2016ja022471-f02-z-.eps

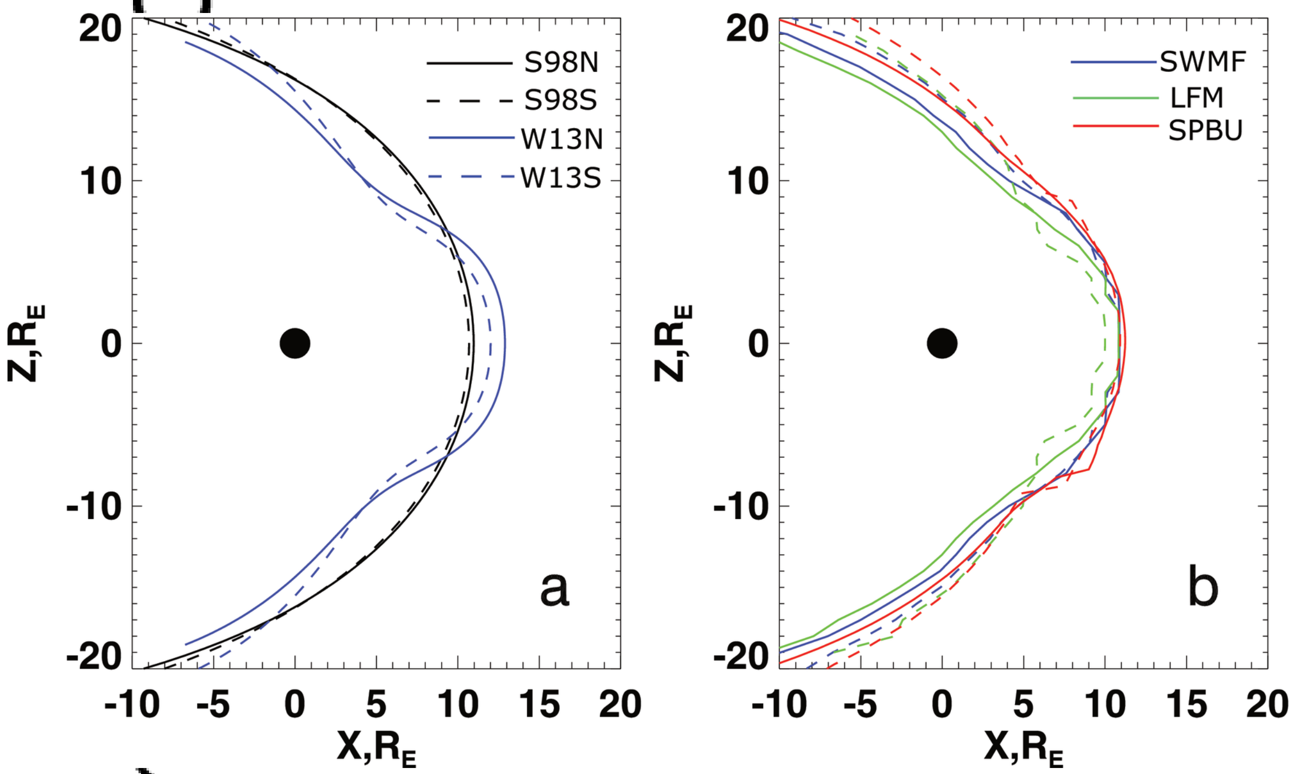

2016ja022471-f03-z-.eps

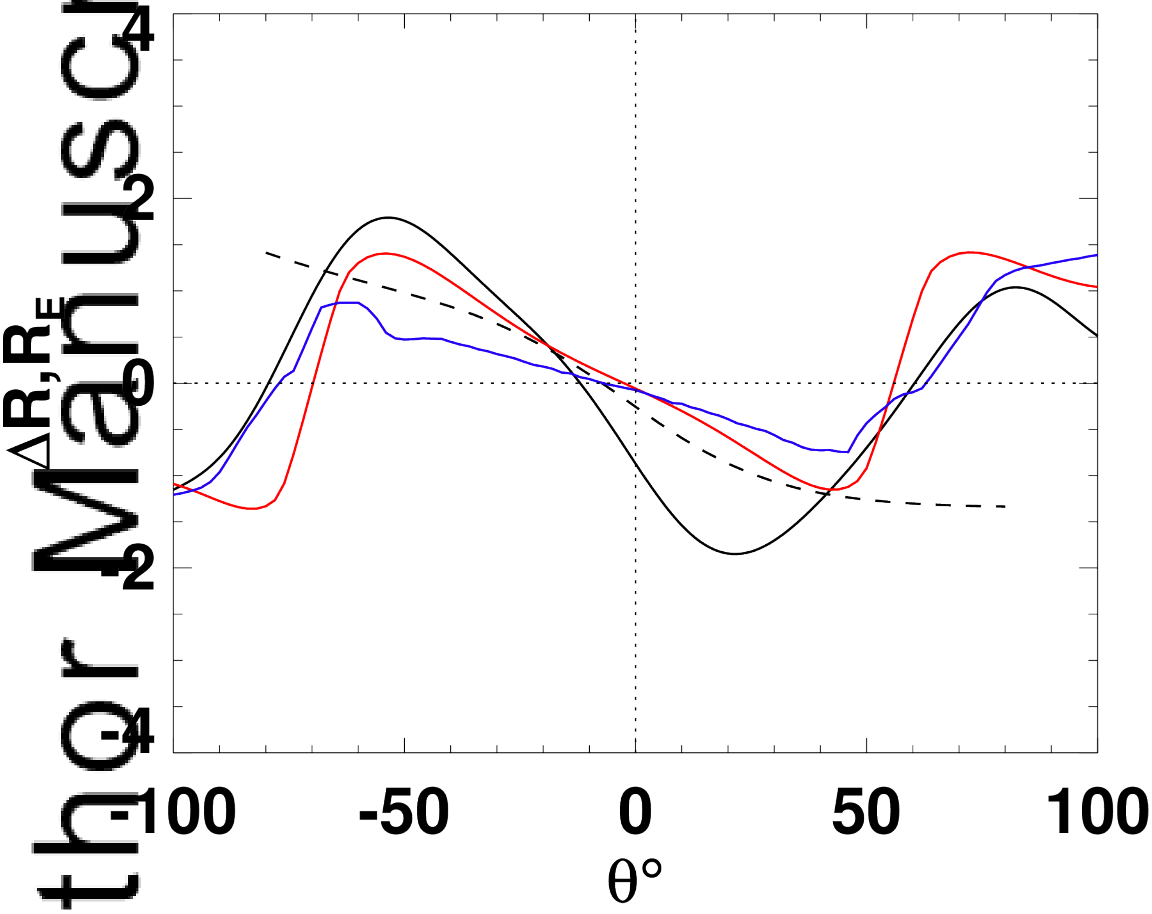

2016ja022471-f04-z-.eps